Coupling of global toroidal Alfvén eigenmodes and reversed shear Alfvén eigenmodes in DIII-D[a)]

M. A. Van Zeeland,[1,b)] M. E. Austin,[2] N. N. Gorelenkov,[3] W. W. Heidbrink,[4] G. J. Kramer,[3] M. A. Makowski,[5] G. R. McKee,[6] R. Nazikian,[3] E. Ruskov,[7] and A. D. Turnbull[1]
[1]*General Atomics, P.O. Box 85608, San Diego, California 92186-5608*
[2]*Fusion Research Center, University of Texas, 1 University Station, Austin, Texas 78712-0263*
[3]*Princeton Plasma Physics Laboratory, P.O. Box 451, Princeton, New Jersey 08543*
[4]*University of California, Irvine, California 92697*
[5]*Lawrence Livermore National Laboratory, Livermore, California 94550*
[6]*University of Wisconsin, 1500 Engineering Drive, Madison, Wisconsin 53706*
[7]*University of California, Irvine, California 92697*

(Received 27 October 2006; accepted 14 December 2006; published online 23 March 2007)

Reversed shear Alfvén eigenmodes (RSAEs) are typically thought of as being localized near the minima in the magnetic safety factor profile, however, their spatial coupling to global toroidal Alfvén eigenmodes (TAEs) has been observed in DIII-D discharges. For a decreasing minimum magnetic safety factor, the RSAE frequency chirps up through that of stable and unstable TAEs. Coupling creates a small gap at the frequency degeneracy point forming two distinct global modes. The core-localized RSAE mode structure changes and becomes temporarily global. Similarly, near the mode frequency crossing point, the global TAE extends deeper into the plasma core. The frequency splitting and spatial structure of the two modes throughout the various coupling stages, as measured by an array of internal fluctuation diagnostics, are in close agreement with linear ideal MHD calculations using the NOVA code. The implications of this coupling for eigenmode stability is also investigated and marked changes are noted throughout the coupling process. © *2007 American Institute of Physics*. [DOI: 10.1063/1.2436489]

I. INTRODUCTION

Alfvén eigenmodes (AEs) in tokamak plasmas are of interest for a variety of reasons. Specifically, their ability to adversely impact fusion performance as well as to cause harm to first wall components by induced fast-ion loss or redistribution has been well documented.[1,2] Additionally, recent experiments touting the positive aspects of Alfvén eigenmodes point to their potential to produce useful modifications of the internal current profile[3] as well as offer diagnostic information about fundamental plasma parameters.[4–6]

Tokamaks operating with reversed central magnetic shear support several types of Alfvén eigenmodes. One of these, localized near minima in the magnetic safety factor ($q_{\min}$), is called the reversed shear Alfvén eigenmode (RSAE) (Refs. 7 and 8) or Alfvén cascade.[5,9] The RSAE is composed primarily of one poloidal harmonic (m). As $q_{\min}$ decreases, the mode transitions to a toroidal Alfvén eigenmode (TAE) with two dominant poloidal harmonics (m and $m-1$). In the zero pressure limit, the RSAE frequency changes as $f_{\mathrm{RSAE}}=[(m-nq_{\min})V_A]/(2\pi q_{\min}R)$,[5,10] where n is the toroidal mode number, V_A is the Alfvén speed, and R is the major radius. Thus, frequency up-chirping for a decreasing $q_{\min}$ is observed. Other effects, due to finite pressure, create nonzero minimum frequencies and have also been shown to be responsible for up and downward chirping RSAE frequencies.[7]

A cartoon illustrating this frequency chirping process is shown in Fig. 1 where several RSAE to TAE transitions for a given n are shown as a function of $q_{\min}$. Interestingly, as the toroidal mode number increases, the number of possible transitions from the RSAE to TAE also increases for a given range of q values. In fact, the RSAE to TAE transition leads to the possibility of having up to $2n$ core-localized TAEs for every integer decrease in $q_{\min}$. Additionally, other global TAEs (GTAE) which are composed of many poloidal harmonics may be present in the same discharges, shown as a dashed line in Fig. 1.

GTAEs and TAEs are characterized by relatively constant frequencies as compared to the rapidly chirping RSAE frequency. Both however, have comparable frequency ranges set by the TAE gap, the center of which is given approximately by $f_{\mathrm{TAE}}=V_A/4\pi qR$. The RSAE frequency chirping through a background of TAE creates several potential instances where the RSAE and TAE or GTAE with the same n can have degenerate frequencies (frequency crossing points in Fig. 1), allowing mode coupling between the two. Coupling similar to this has been inferred from a combination of magnetic measurements and ideal-MHD modeling on JT-60U, and more recently JET, where frequency chirping core-localized TAEs were found to couple to global TAEs.[11,12]

This paper presents the first internal measurements of the coupling of RSAEs to TAEs. The coupling creates a small gap at the frequency crossing point forming two distinct global modes that represent odd and even parity mixed combinations of the RSAE and TAE. The spatial structure of the two modes and frequency splitting, as measured by an array of internal fluctuation diagnostics, are in agreement with lin-

[a)]Paper BI1 4, Bull. Am. Phys. Soc. **51**, 21 (2006).
[b)]Invited speaker.

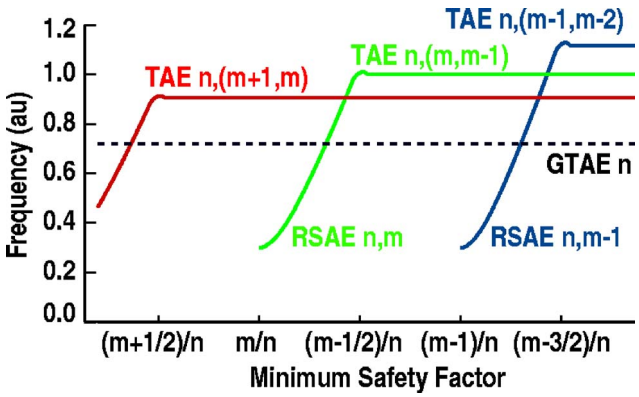

FIG. 1. Cartoon illustrating several RSAE frequency chirps and the resultant TAEs (solid) as a function of q_{min} for a reversed-shear discharge, n and m are toroidal and poloidal mode number, respectively. (Dashed) Possible GTAE frequency.

ear ideal MHD calculations using the NOVA code.[13,14]

The coupling of these modes alters their individual stability properties as well as their potential to cause fast ion transport. TAEs have been shown to cause severe losses of injected neutral beam ions and the subsequent destruction of several in-vessel components.[15] On the other hand, as of yet, no experimental evidence clearly shows core-localized RSAEs alone as being the cause for fast ion losses. In fact, several theoretical investigations predict little effect on the fast ion population due solely to core-localized modes.[16] Recent measurements of the RSAE during its transition to a TAE and the subsequent effect on neutron production show marked decreases in neutron emission at the point of transition to the more global TAE.[17] The coupling of the RSAE to the TAE may create instances where the mixed state can actually cause significant transport whereas the RSAE by itself possibly may not.

II. MODE COUPLING: EXPERIMENT AND SIMULATION

A. Spectral characteristics

The primary discharge of interest in this study is analyzed during the current ramp phase when 5 MW, 78 kV, unbalanced co-going, sub-Alfvénic ($V_B/V_A \approx 0.4$), neutral deuterium beams are injected into the plasma. The central β (plasma pressure/magnetic field pressure) is increasing during this period, and there is an off-axis minimum in the magnetic safety factor. The electron density is relatively low $\approx 2\times 10^{13}$ cm^{-3}, making the fast-ion pressure roughly half of the total plasma pressure according to TRANSP (Ref. 18) analysis. Several fluctuation diagnostics show a variety of Alfvénic activity in this discharge; each, however, has a different instrument function and preferred sensitivity to particular types of AEs.[19] This makes it useful to look across several diagnostics for a clear picture of what modes are present in the plasma at a given time. Shown in Fig. 2 is a crosspower spectrum of a beam emission spectroscopy (BES) (Ref. 20) channel located near q_{min} and a vertical CO_2 interferometer chord.[21] Previous analysis has identified the modes chirping up in frequency as RSAEs and the series of relatively constant frequency modes as TAEs.[22] Over the

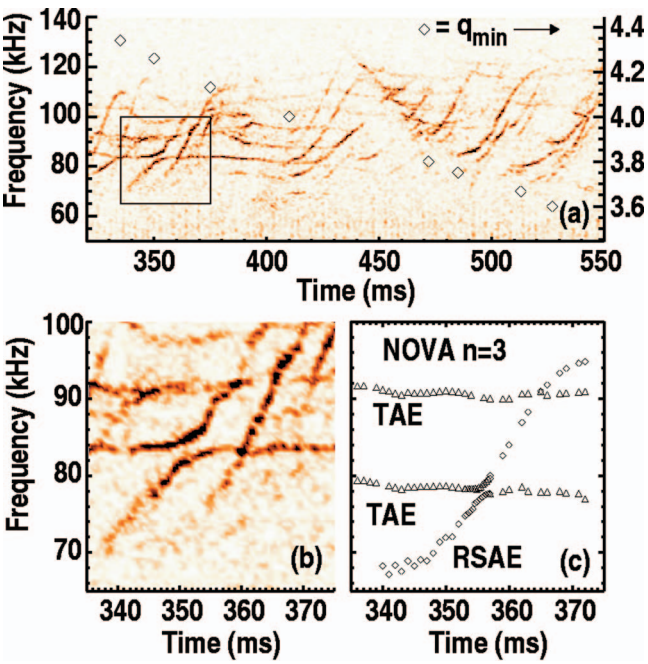

FIG. 2. (Color) Discharge 122117. (a) Cross power of a BES channel near q_{min} and a vertical CO_2 interferometer chord. Diamonds indicate values of q_{min} from RSAE timing in combination with MSE measurements. (b) Expanded region of (a). (c) NOVA simulated frequencies for $n=3$ RSAE and TAEs.

time window shown, the RSAE spectral behavior is prototypical for q_{min} decreasing and crossing an integer value ($q_{min}=4$) at approximately $t=410$ ms.[19] Plotted in Fig. 2(a) (diamonds) are values of q_{min} derived from the RSAE activity in combination with motional Stark effect (MSE) measurements.[23] Behavior which does not fit the simple model of many different n RSAE are the occasional gaps in the observed mode amplitudes and frequency evolution. Such "gaps" are displayed more clearly in Fig. 2(b) where an expanded region of Fig. 2(a) is shown. The mode at approximately 84 kHz is an $n=3$ global TAE according to detailed comparisons between electron cyclotron emission (ECE) measurements and ideal MHD simulations,[22] and the mode chirping up from approximately 70 kHz to 100 kHz is an $n=3$ RSAE, where the toroidal mode number has been obtained from a toroidal array of Mirnov loops. The particular region of interest occurs near $t=352$ ms, $f=83$ kHz and corresponds to the point at which these two modes should have degenerate frequencies. Such frequency crossing avoidance is a signature of mode-mode coupling and is reminiscent of coupled oscillators in classical and quantum mechanics as well as the previous work by Kramer *et al.* in which the coupling of two TAEs was investigated using external magnetic measurements.[11]

Figure 2(c) shows the calculated mode frequency temporal evolution for two $n=3$ TAEs and one $n=3$ RSAE found using the ideal MHD code NOVA for this discharge.[13,14] As inputs, NOVA uses the measured spatial profiles of electron density, electron temperature, safety factor, ion temperature, and toroidal rotation[24] obtained from Thomson scattering, MSE, and charge exchange recombination (CER) measurements. The input equilibria are obtained from EFIT (Ref. 25)

equilibrium magnetic flux reconstructions that use MSE, magnetics, and thermal plasma pressure data. The safety factor profiles used in the MHD analysis were translated slightly from those derived by the MSE measurements so as to have $q_{\min}$ coincide with that inferred from the temporal evolution of Alfvén cascade frequencies;[19] all changes were less than 5% of the measured value and well within the roughly 10% estimated error of MSE measurements. Throughout the time window shown in Figs 2(b) and 2(c), $q_{\min}$ is linearly decreasing in time from $q_{\min}=4.34$ at $t=335$ ms to $q_{\min}=4.13$ at $t=375$ ms.

Several eigenmodes found in this case can be classified by the radial dependence of the envelope of their poloidal harmonics. The first TAE solution is shown with eigenfrequency $f\approx 90$ kHz and represents the fundamental, lowest radial envelope solution. The second TAE solution is also shown, which corresponds to a radial envelope with one radial node and $f\approx 80$ kHz. Another TAE solution at $f\approx 73$ kHz corresponding to a second radial harmonic was found, but it is not shown. The discrete points in Fig. 2(c) represent individual runs of the NOVA code at each value of $q_{\min}$, the temporal spacing of which was decreased near the frequency degeneracy point in order to unambiguously resolve the crossing frequency avoidance of the first radial harmonic global TAE and the RSAE. The MHD simulations clearly reproduce many of the major features of the experimental data shown in Fig. 2(b), i.e., crossing avoidance, several TAEs, and the frequency chirping of the RSAE. The exact time where the crossing avoidance occurs differs between Figs. 2(b) (experiment) and 2(c) (simulation), $t\approx 352$ ms and $t\approx 355$ ms, respectively. This difference could be the cumulative result of inaccuracies in the measured input profiles as well as γ (the ratio of specific heats), which was taken as the canonical value 5/3. The RSAE frequency in particular is very sensitive to $q_{\min}$ and γ as was mentioned in Ref. 22. An additional mode coupling occurs when the RSAE crosses the TAE near $f\approx 90$ kHz. Although not as clear as the coupling with the ≈80 kHz mode, some evidence for this coupling exists in Fig. 2(b). Qualitatively, this may be expected from the fact that the calculated eigenmodes are found to have less radial overlap for the 90 kHz crossing as compared to the 80 kHz.

B. Spatial characteristics

The $n=3$ Alfvén continuum for $t=353$ ms is shown in Fig. 3 along with the experimental profiles of electron temperature (T_e), ion temperature (T_i), electron density (n_e), and safety factor (q). The radial coordinate used is ρ, the normalized square-root of the toroidal flux. Implicit in Fig. 3(b) is the toroidal rotation frequency which is roughly 3.7 kHz on axis and 3.1 kHz at $q_{\min}$. The horizontal lines in Fig. 3(b) indicate where the predicted displacement (ξ) is above $1/e$ of its maximum value for the RSAE and lower frequency TAE of Fig. 2(c). The solid curve is the Alfvén continuum. The RSAE is peaked near $q_{\min}$ as expected and the TAE is more global and extends over a wider region. Both modes are located in the TAE gap and neither intersects the continuum significantly.

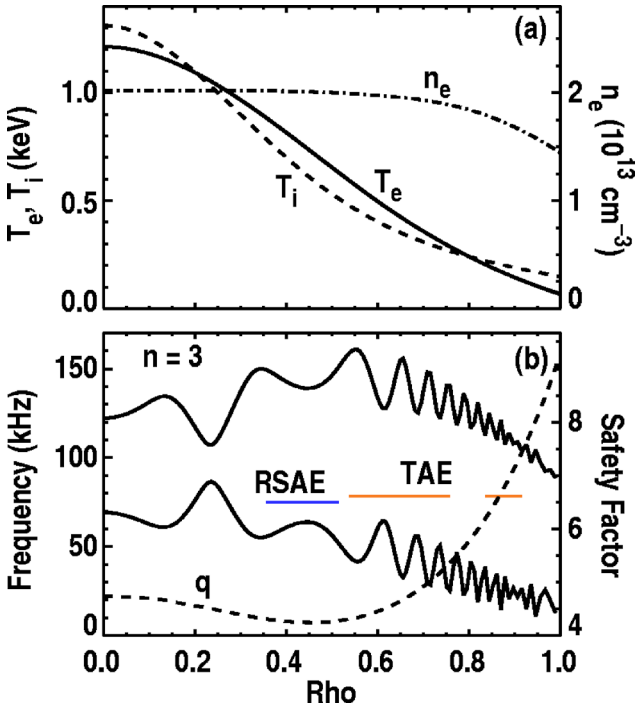

FIG. 3. Discharge 122117, $t=353$ ms (a) Experimental profiles of electron density (n_e), electron temperature (T_e), and ion temperature (T_i). (b) NOVA calculated $n=3$ Alfvén continuum. Frequencies of RSAE (blue) and TAE (gold) from Fig. 2 are shown as lines plotted where the displacement is above $1/e$ of its max. Safety factor is overplotted (dashed line). $B_T=2.01$ T, $R_m=1.63$ m, $a=0.61$ m, elongation=1.53, triangularity=0.24.

As the RSAE chirps up in frequency and mixes with the TAE, both modes' spatial eigenfunctions change drastically. This process is depicted in Fig. 4, where the predicted displacement mode structure is shown for several stages of the coupling, i.e., *before*, *during*, and *after* frequency crossing avoidance. The displacement plots show the largest ten poloidal harmonics of each eigenmode on the outboard midplane. Before mixing, the global TAE is composed of several poloidal harmonics and has essentially two main peaks out of phase with each other while the RSAE has primarily one poloidal harmonic and is much more radially localized. At the position of minimum frequency separation the two modes are highly coupled with the resultant eigenfunctions being linear combinations of the two individual modes. The upper frequency mode is the in-phase addition of the RSAE and TAE and the lower frequency mode is the out-of-phase combination. After the crossing point both the RSAE and TAE return to nearly their original structure, with the exception that the TAE has undergone a 180° phase shift. Experimentally, this final phase shifted TAE would be indistinguishable from the original TAE. Throughout this process, independent of the mode coupling, the RSAE is undergoing a transition to a TAE (as described in the Introduction) and as a result a second poloidal harmonic is becoming more apparent. At the end of its frequency up chirp, the RSAE has two dominant poloidal harmonics which are of equal magnitude (not shown).

Verification of the evolution of the spatial eigenfunction during the coupling process is provided by the DIII-D ECE

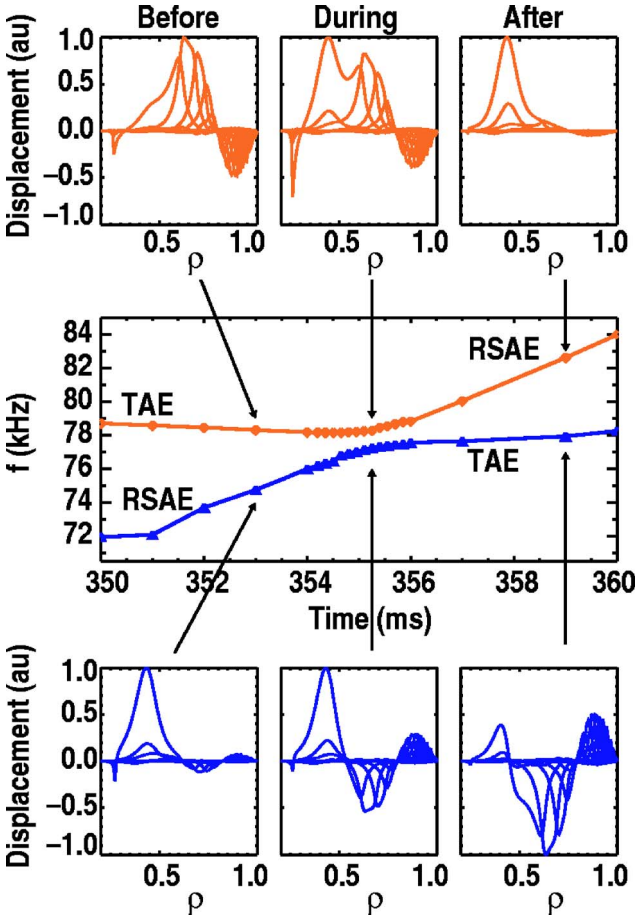

FIG. 4. MHD simulation. Field line displacement of the upper and lower frequency $n=3$ modes *before*, *during*, and *after* frequency crossing avoidance of Fig. 2. The largest ten poloidal harmonics are shown.

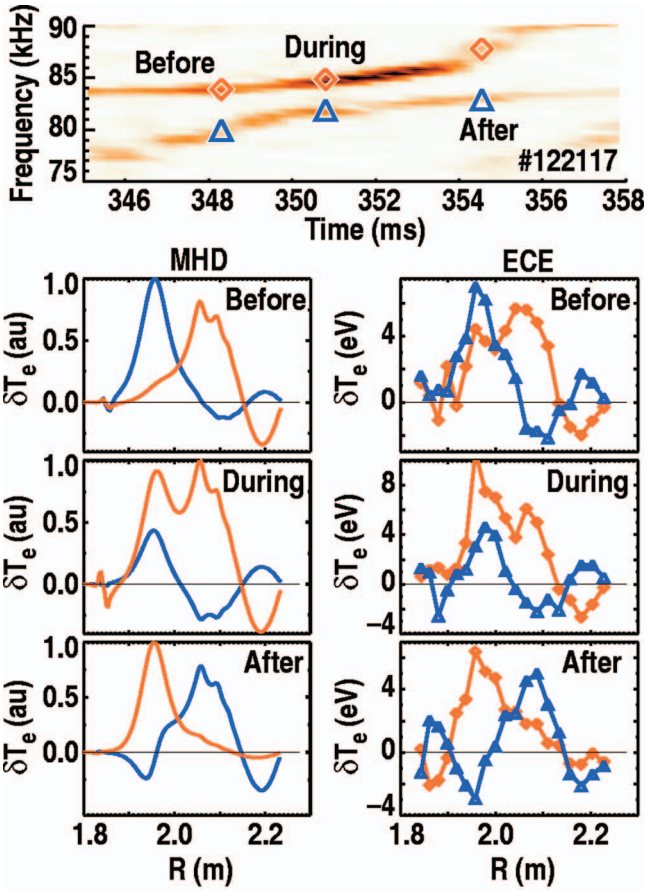

FIG. 5. (Color) (Top panel) Enlarged region of Fig. 2(a), diamonds and triangles indicate frequencies of corresponding modes in ECE column. (Left column) NOVA predicted temperature perturbation corresponding to Fig. 4 *before*, *during*, and *after* frequency crossing avoidance at simulation times $t=355.25-2.5$, $t=355.25$, and $t=355.25+3.75$ ms, respectively. Gold/blue is the higher/lower frequency mode. (Right column) ECE data showing measured temperature perturbation *before*, *during*, and *after* frequency crossing avoidance of the higher/lower frequency mode (gold diamonds/blue triangles). Experimental times are $t=350.8-2.5$, $t=350.8$, $t=350.8+3.75$ ms.

radiometer which measures electron temperature fluctuations resulting from the magnetic field line displacement and adiabatic compression of shear Alfvén modes. The newly upgraded ECE heterodyne radiometer on DIII-D obtains detailed structural information on AEs using a total of 40 radially spaced channels across the plasma midplane.[26] In order to compare ECE measurements with MHD calculations, a synthetic diagnostic approach was taken in which the NOVA predicted displacement (ξ) was used to calculate an electron temperature perturbation from

$$\frac{\delta T_e}{T_e} = -(\gamma - 1)\nabla \cdot \xi - \xi \cdot \frac{\nabla T_e}{T_e}, \tag{1}$$

(Refs. 14 and 27). The synthetic diagnostic essentially averages the predicted temperature perturbation over the finite ECE collection volume assuming a Gaussian beam profile in the vertical and toroidal directions with a beam waist set by the microwave viewing optics and a notch-like acceptance function in the radial direction to simulate the rf filters used.[22]

Shown in the left column of Fig. 5 are the predicted temperature perturbation eigenfunctions corresponding to the displacement plots of Fig. 4, with the gold and blue representing the upper and lower frequency modes, respectively. The predicted temperature perturbations are in arbitrary units due to the fact that NOVA is a linear code and is only capable of predicting the shape of the perturbation. The ratio of the upper and lower frequency mode amplitude has been scaled by the ratio of the actual ECE measured peak mode amplitudes. The right column of Fig. 5 shows the corresponding temperature perturbation eigenmode measured using ECE. Due to the fact that the crossover occurs at different times experimentally as compared to the NOVA simulation, for the sake of comparison, the middle (*during*) time-slice corresponds to the point of minimum frequency separation between the upper and lower frequency modes (t_m), with $t_m=350.8$ ms in the experiment and $t_m=355.25$ ms in the simulations. The *before* and *after* times are then taken with respect to this time at $t=t_m-2.5$ ms and $t=t_m+3.75$ ms, respectively. The ECE eigenmodes shown are $\delta T_e=A\cos(\phi)$ where the amplitude (A) and phase (ϕ) are taken from a FFT and ϕ is relative to the phase of the largest amplitude channel.

The ECE data clearly display many of the characteristics of the MHD predictions and gives physical amplitudes to the

eigenmodes themselves. The *during* plot shows a marked decrease in the lower frequency peak amplitude and an increase in the amplitude of the upper frequency coupled mode. This is consistent with the modes being a linear combination of the RSAE (blue) and TAE (gold) in the *before* panel formed simply by the weighted addition/subtraction of the two, i.e., the upper/lower frequency modes, respectively. Physically, this frequency degeneracy removal by the linear combination of eigenfunctions is strikingly similar to the quantum mechanics problem of two adjacent potential wells with solutions coupled through tunneling.[10,28,29]

C. Stability properties

Throughout the coupling process the modes that were initially discrete RSAE and TAE combine to form global AEs as shown in the previous section. It is expected that these mixed global modes may have different stability properties as a result of their new radially extended structure. For instance, in the case of a core-localized TAE interacting with a global TAE on JT-60U, the authors point out that the global mode intersected the Alfvén continuum at the edge. This caused significant continuum damping and, when the coupling occurs, the chirping mode was subject to the increased damping of the global mode resulting in a decrease in the observed mode amplitude.[11] The modes presented here experience little continuum damping; however, electron Landau and electron collisional damping are found to be dominant.

The stability properties of these modes have been investigated using the kinetic extension of the NOVA code called NOVA-K, which gives both the damping and an estimate of the growth rate using a δW method that includes finite Larmor radius effects.[30] The drive is due to energetic beam ions, injected into the plasma almost tangentially. At injection the average pitch angle, as modeled by TRANSP, equals $\chi_0 \equiv v_\parallel/v = 0.7$, whereas the width of the distribution function in pitch angle was $\delta\chi = 0.12$. The NOVA-K model of the distribution function evolution as beam ions slow down is described in Ref. 31.

Shown in Fig. 6 are plots of the calculated mode frequencies (for reference) Fig. 6(a), damping rate γ_{damp} (sum of electron collisional and electron Landau) Fig. 6(b), drive γ_{drive} Fig. 6(c), and $\gamma_{\text{drive}}/\gamma_{\text{damp}}$ Fig. 6(d). There is a significant effect on the damping of both the RSAE and TAE. At the point of minimum frequency separation, both modes have approximately the same damping; this corresponds to an increase in that of the TAE and a decrease for the RSAE. Likewise, the drive also reaches approximately the same value for the two eigenmodes during the time of minimum frequency separation, which corresponds to an increased drive for the TAE and a decreased drive for the RSAE. For the TAE this may be understood in that the fast ion pressure gradient is largest near $\rho = 0.3$ and is down to approximately 25% its maximum value where the TAE peaks. By coupling to the RSAE, which peaks near $\rho = 0.4$, the mode reaches deeper in the plasma core and closer to the region where fast ion pressure profile is peaked. It is noteworthy that both the drive and damping shown in Figs. 6(c) and 6(d) are large (up to 10%), which pushes the NOVA-K perturbative analysis to

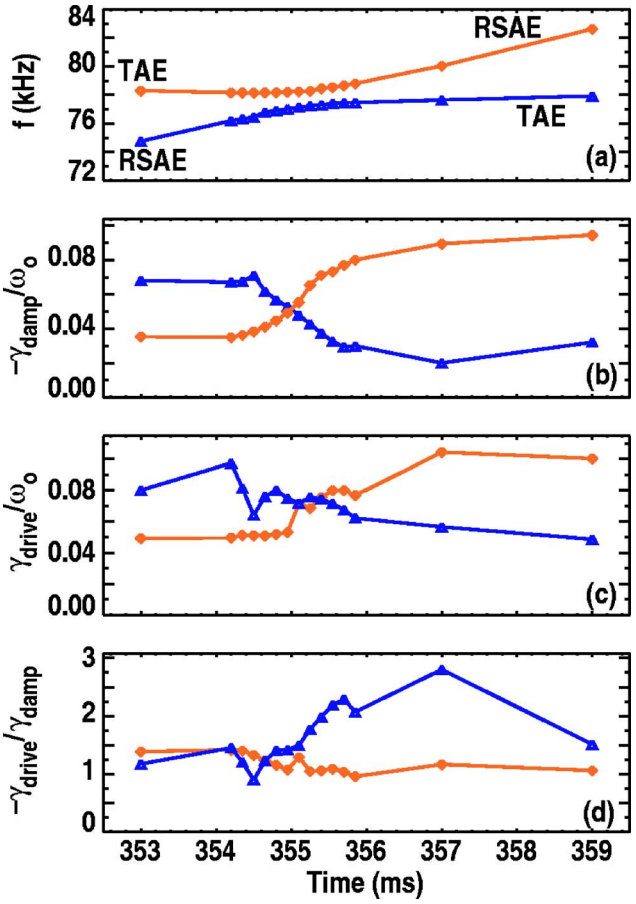

FIG. 6. Results from the NOVA-K code for discharge 122117. (a) Frequency evolution during crossover avoidance, (b) sum of electron collisional and Landau damping γ_{damp} normalized to mode frequency, (c) neutral beam ion drive γ_{drive} normalized to mode frequency, and (d) ratio of drive to damping $\gamma_{\text{drive}}/\gamma_{\text{damp}}$ for the modes in (a).

the limit of its applicability. A nonperturbative analysis may be appropriate. However, even in this case of strong drive and damping the ideal MHD RSAE and TAE structures appear to be sufficient as shown in the previous section where remarkable agreement is found with eigenmode measurements, supporting the applicability of the perturbative theory used.

The net result of the drive and damping is shown in Fig. 6(d) where the ratio, $\gamma_{\text{drive}}/\gamma_{\text{damp}}$ is given. The net relative drive of the RSAE is seen to remain somewhat constant with the exception of a large temporary decrease around $t = 354.5$ ms. For the TAE, $\gamma_{\text{drive}}/\gamma_{\text{damp}}$ decreases slightly then increases significantly after crossover avoidance. For these calculations, the drive increases linearly with central fast-ion beta which was fixed at 0.69% as compared to the total central beta of 1.02%. The fast ion pressure profile was calculated using the TRANSP code which assumes neoclassical confinement. For the purposes of comparing the relative changes between eigenmodes and showing that there is a change in the stability through the coupling process, this presents no problem; however, Fig. 6(d) predicts some of these eigenmodes to be only marginally stable/unstable. Further analysis is required to resolve this discrepancy since both modes are observed in experiment and are clearly unstable

throughout the coupling process. Indeed, for these discharges with multiple Alfvén eigenmodes, the volume averaged neutron emission is approximately half the classical value predicted by TRANSP (Ref. 32) making use of the calculated fast ion pressure profile questionable.

III. DISCUSSION AND CONCLUSION

In addition to the calculations and data presented thus far for the coupling of an unstable RSAE and TAE, much evidence exists both experimentally and theoretically for coupling of the frequency chirping RSAE to stable TAEs/GTAEs. Simulations carried out for the same time window as Fig. 2(c) and $n=2$ and $n=4$ predict the coupling to several GTAEs just as for the $n=3$ modes presented, with the exception that no $n=2$ or $n=4$ GTAEs are obvious in the experimental measurements. However, analysis of multichannel ECE data confirms that throughout their respective frequency chirps, most of the other RSAEs also temporarily take on a global structure such as that shown in Fig. 5. Interestingly, a sign of this is the momentary appearance of RSAE activity on magnetic pickup measurements which tend to only be sensitive to the modes when they have a significant amplitude at the plasma edge. An example of this can be seen in Ref. 22, Fig. 1(c) where a windowed power spectrum of Mirnov coil data for the same discharge of this paper is presented. Also, recently it has been found that analogous modes to the RSAE can exist in higher order gaps in the Alfvén continuum.[33] These modes, like the RSAE, chirp in frequency and as a result will likely be subject to the same type of coupling as described here, except with higher frequency Alfvén eigenmodes such as the NAE (triangularity induced Alfvén eigenmode).

In summary, measurements of the coupling of RSAEs to TAEs in DIII-D reversed magnetic shear plasmas have been presented. The measured mode structures, frequencies, and frequency splitting throughout the coupling process are in close agreement with ideal MHD simulations. It has been observed that the core-localized RSAE can temporarily gain a global mode structure whereby its stability properties as well as a potential to cause fast ion transport is altered. Phenomenologically, the plasma discussed here also shows flattening of the central fast-ion pressure profile during periods of strongest Alfvénic activity.[32] However, due to insufficient time resolution of the necessary diagnostics to assess the impact on injected beam ions during the relatively short coupling event, no data have been presented to this end. Future work should focus on the degree to which Alfvénic mode coupling affects fast ion confinement. This coupling process may be particularly important in future burning plasma experiments where moderate to high-n Alfvén modes are predicted to be unstable. The number of possible eigenmodes increases with n, therefore a chirping RSAE with higher-n will have more opportunities to couple to TAEs possibly resulting in an unexpected increase in global Alfvén eigenmode activity.

ACKNOWLEDGMENTS

The authors wish to thank Professor L. Chen, and Dr. F. Volpe for many interesting and useful discussions as well as Dr. S. E. Sharapov for sharing recent JET data exhibiting similar RSAE coupling behavior.

This work was supported by the U.S. Department of Energy under Contract Nos. DE-FC02-04ER54698, DE-FG03-97ER54415, DE-AC02-76CH03073, SC-G903402, W-7405-ENG-48, and DE-FG02-89ER53296, and in part by an appointment to the U.S. Department of Energy Fusion Energy Postdoctoral Research Program administered by the Oak Ridge Institute for Science and Education.

[1] K. L. Wong, Plasma Phys. Controlled Fusion **41**, R1 (1999).
[2] K. Shinohara, Y. Kusama, M. Takechi, A. Morioka, M. Ishikawa, N. Oyama, K. Tobita, T. Ozeki, S. Takeji, S. Moriyama *et al.*, Nucl. Fusion **41**, 603 (2001).
[3] K. L. Wong, R. Budny, R. Nazikian, C. C. Petty, C. M. Greenfield, W. W. Heidbrink, and E. Ruskov, Phys. Rev. Lett. **93**, 085002–1 (2004).
[4] H. A. Holties, J. P. Goedbloed, G. T. A. Huysmans, and W. Kerner, Plasma Phys. Controlled Fusion **39**, 73 (1997).
[5] H. L. Berk, D. N. Borba, B. N. Breizman, S. D. Pinches, and S. E. Sharapov, Phys. Rev. Lett. **87**, 185002 (2001).
[6] M. F. Nave, D. Borba, R. Galvao, S. Hacquin, B. Alper, C. Challis, S. Gerasimov, N. Hawkes, J. Mailloux, S. Sharapov *et al.*, Rev. Sci. Instrum. **75**, 4274 (2004).
[7] G. J. Kramer, N. N. Gorelenkov, R. Nazikian, and C. Z. Cheng, Plasma Phys. Controlled Fusion **46**, L23 (2004).
[8] Y. Kusama, H. Kimura, T. Ozeki, M. Saigusa, G. J. Kramer, T. Oikawa, S. Moriyama, M. Nemoto, T. Fukita, K. Tobita *et al.*, Nucl. Fusion **38**, 1215 (1998).
[9] S. E. Sharapov, B. Alper, H. L. Berk, D. N. Borba, B. N. Breizman, C. D. Challis, A. Fasoli, N. C. Hawkes, T. C. Hender, J. Mailloux, S. D. Pinches, and D. Testa, Phys. Plasmas **9**, 2027 (2002).
[10] B. N. Breizman, H. L. Berk, M. S. Pekker, S. D. Pinches, and S. E. Sharapov, Phys. Plasmas **10**, 3649 (2003).
[11] G. J. Kramer, C. Z. Cheng, G. Y. Fu, Y. Kusama, R. Nazikian, T. Ozeki, and K. Tobita, Phys. Rev. Lett. **83**, 2961 (1999).
[12] N. P. Young, S. E. Sharapov, V. M. Nakariakov, and JET EFDA contributors, Plasma Phys. Controlled Fusion **48**, 295 (2006).
[13] C. Z. Cheng and M. S. Chance, J. Comput. Phys. **71**, 124 (1987).
[14] C. Z. Cheng, Phys. Rep. **211**, 1 (1992).
[15] H. H. Duong, W. W. Heidbrink, T. W. Petrie, R. Lee, R. A. Moyer, and J. G. Watkins, Nucl. Fusion **33**, 749 (1993).
[16] J. Candy, H. L. Berk, B. N. Breizman, and F. Porcelli, Phys. Plasmas **6**, 1822 (1999).
[17] M. Takechi, A. Fukuyama, M. Ishikawa, C. Z. Cheng, K. Shinohara, T. Ozeki, Y. Kusama, S. Takeji, T. Fujita, T. Oikawa *et al.*, Phys. Plasmas **12**, 082509 (2005).
[18] R. V. Budny, Nucl. Fusion **34**, 1247 (1994).
[19] M. A. Van Zeeland, M. E. Austin, T. N. Carlstrom, T. Deterly, D. K. Finkenthal, C. T. Holcomb, R. J. Jayakumar, G. J. Kramer, M. A. Makowski, G. R. McKee *et al.*, Nucl. Fusion **46**, S880 (2006).
[20] D. K. Gupta, R. J. Fonck, G. R. McKee, D. J. Schlossberg, and M. W. Shafer, Rev. Sci. Instrum. **75**, 3493 (2004).
[21] M. A. Van Zeeland, G. J. Kramer, R. Nazikian, H. L. Berk, T. N. Carlstrom, and W. M. Solomon, Plasma Phys. Controlled Fusion **47**, L31 (2005).
[22] M. A. Van Zeeland, G. J. Kramer, M. E. Austin, R. L. Boivin, W. W. Heidbrink, M. A. Makowski, G. R. McKee, R. Nazikian, W. M. Solomon, and G. Wang, Phys. Rev. Lett. **97**, 135001 (2006).
[23] C. T. Holcomb, M. A. Makowski, R. J. Jayakumar, S. L. Allen, R. M. Ellis, R. Geer, D. Behne, K. L. Morris, L. G. Seppala, and J. M. Moller, Rev. Sci. Instrum. **77**, 10E506 (2006).
[24] G. J. Kramer, R. Nazikian, B. Alper, M. de Baar, H. L. Berk, G.-Y. Fu, N. N. Gorelenkov, G. McKee, S. D. Pinches, T. L. Rhodes *et al.*, Phys. Plasmas **13**, 056104 (2006).

[25]L. L. Lao, H. E. St John, R. D. Stambaugh, A. G. Kellman, and W. Pfeiffer, Nucl. Fusion **25**, 1611 (1985).
[26]M. E. Austin and J. Lohr, Rev. Sci. Instrum. **74**, 1457 (2003).
[27]F. F. Chen, *Introduction to Plasma Physics and Controlled Fusion* (Plenum, New York, 1984).
[28]L. Chen, N. N. Gorelenkov, and F. Volpe (private communication, 2006).
[29]Roscoe B. White, *Asymptotic Analysis of Differential Equations* (Imperial College, London, 2005).
[30]N. N. Gorelenkov, C. Z. Cheng, and G. Y. Fu, Phys. Plasmas **6**, 2802 (1999).
[31]N. N. Gorelenkov, H. L. Berk, and R. Budny, Nucl. Fusion **45**, 226 (2005).
[32]W. W. Heidbrink, in Proceedings of the 21st IAEA Fusion Energy Conference, Chengdu, China (2006).
[33]G. J. Kramer and G. Y. Fu, Plasma Phys. Controlled Fusion **48**, 1285 (2006).